Received: 1 July 2022 | Revised: 27 July 2022 | Accepted: 2 August 2022

DOI: 10.1002/smm2.1149

RESEARCH ARTICLE

SmartMat Open Access WILEY

Insights into enhanced electrochemiluminescence of a multiresonance thermally activated delayed fluorescence molecule

Liuqing Yang[1] | **Lihui Dong**[1,2] | **David Hall**[3,4] | **Mahdi Hesari**[1] | **Yoann Olivier**[5] | **Eli Zysman-Colman**[3] | **Zhifeng Ding**[1]

[1]Department of Chemistry, Western University, Ontario, London, Canada

[2]Guangxi Key Laboratory of Petrochemical Resource Processing and Process Intensification Technology, School of Chemistry and Chemical Engineering, Guangxi University, Nanning, China

[3]Organic Semiconductor Centre, EaStCHEM School of Chemistry, University of St Andrews, St Andrews, Fife, UK

[4]Laboratory for Chemistry of Novel Materials, University of Mons, Mons, Belgium

[5]Laboratory for Computational Modeling of Functional Materials, Namur Institute of Structured Matter, University of Namur, Namur, Belgium

Correspondence
Zhifeng Ding, Department of Chemistry, Western University, Ontario N6A 3K7, London, Canada.
Email: zfding@uwo.ca

Yoann Olivier, Laboratory for Computational Modeling of Functional Materials, Namur Institute of Structured Matter, University of Namur, Rue de Bruxelles, 615000 Namur, Belgium.
Email: yoann.olivier@unamur.be

Eli Zysman-Colman, Organic Semiconductor Centre, EaStCHEM School of Chemistry, University of St Andrews, St Andrews, Fife KY16 9ST, UK.
Email: eli.zysman-colman@st-andrews.ac.uk

Funding information
Walloon Region, Grant/Award Number: n1117545; Leverhulme Trust, Grant/Award Numbers: RPG-2016047, SRF\R1\201089; Natural Sciences and Engineering Research Council Canada, Grant/Award Numbers: DG RGPIN-2018-06556, SPG STPGP-2016-493924; Fonds de la Recherche Scientifiques de Belgique,

Abstract

The electrochemiluminescence (ECL) behavior of a multiresonance thermally activated delayed fluorescence molecule has been investigated for the first time by means of ECL-voltage curves, newly designed ECL-time observatory, and ECL spectroscopy. The compound, **Mes_3DiKTa**, shows complex ECL behavior, including a delayed onset time of 5 ms for ECL generation in both the annihilation pathway and the coreactant route, which we attribute to organic long-persistent ECL (OLECL). Triplet-triplet annihilation, thermally activated delayed fluorescence and uncompensated solution resistance cannot be ruled out as contributing mechanisms to the ECL. A very long ECL emission decay was attributed to OLECL as well. The absolute ECL efficiencies of **Mes_3DiKTa** were enhanced and reached 0.0013% in annihilation route and 1.1% for the coreactant system, which are superior to those of most other organic ECL materials. It is plausible that ECL materials with comparable behavior as **Mes_3DiKTa** are desirable in applications such as ECL sensing, imaging, and light-emitting devices.

KEYWORDS
electrochemiluminescence, multiresonant thermally activated delayed fluorescence, organic long-persistent electrochemiluminescence, triplet-triplet annihilation

Liuqing Yang and Lihui Dong contributed equally to this study.

Grant/Award Numbers: 2.5020.11, F.4534.21; Engineering and Physical Sciences Research Council, Grant/Award Number: EP/P010482/1

1 | INTRODUCTION

Electrochemiluminescence (ECL), also termed as electrogenerated chemiluminescence, is a light-emitting process induced and well controlled by electrochemistry in the vicinity of a working electrode,[1–3] in which highly active radical species (polarons) electrochemically generated, undergo electron transfer to form excitons that emit light upon relaxation to ground state.[1,2] Annihilation ECL is a process whereby the electron transfer occurs between radical ions electrogenerated from the same ECL material to produce excitons, while coreactant ECL requires the use of a sacrificial oxidant or reductant whose electrically generated radical interacts with the ECL luminophore polaron to produce the exciton.[1,2] Intelligently combined with electrochemistry and chemiluminescence, ECL has wide application within the fields of sensing and imaging.[4–8] Numerous classes of ECL luminophores (ECLphores) have been reported and their ECL mechanisms studied, including phosphorescent metal complexes,[9–11] organic molecules[12–14] and nanomaterials.[15–19] For example, $[Ru(bpy)_3]^{2+}$, the most widely employed ECLphore, is usually used as the gold standard to determine relative ECL efficiency.[19–22] However, the absolute ECL efficiency of $[Ru(bpy)_3]^{2+}$ is still quite low (0.0019% in a potentiodynamic process or ~5% at a rotating disk-ring electrode), reflecting its low photoluminescence quantum yield ($\phi_{PL} = 9.5\%$ in degassed MeCN).[21,22] The low quantum efficiency of many ECL materials significantly limits their use in practical applications.

The ECL efficiency is governed in part by the electrochemical stability of the radical cations and anions that are formed in the vicinity of the electrodes such that these species do not degrade before their diffusion and recombination to produce excitons.[21–24] As with electroluminescent devices such as organic light-emitting diodes and light-emitting electrochemical cells, the ECL efficiency with which the generated excitons are converted to light depends on the nature of the emitter. For fluorescent emitters, only singlet excitons can produce light, thus limiting the maximum ECL efficiency to 25%. For phosphorescent emitters, singlet excitons are rapidly converted to triplets via intersystem crossing (ISC) before light emission from the triplet state.[25] Thus, for phosphorescent compounds the maximum ECL efficiency is 100%.

ECL has also been demonstrated to be produced via two other processes, both of which involve the conversion of triplet excitons into singlet excitons: triplet-triplet annihilation (TTA) and thermally activated delayed fluorescence (TADF).[26–29] TTA materials produce light with a maximum efficiency of 62.5%, due to the requirement for two triplet excitons to bimolecularly recombine to form a higher energy singlet exciton and a molecule in its ground state.[29] At the concentrations typically used in ECL and TTA is a plausible mechanism for compounds with sufficiently long-lived triplet excitons. TADF compounds also can convert up to 100% of the generated excitons into light. This is possible due to the very small singlet-triplet energy gap (ΔE_{ST}) that permits endothermic up-conversion of triplet excitons into singlet excitons via reverse ISC (RISC).[29] TADF compounds typically show dual emission, with a fast nanosecond prompt fluorescence due to as-formed singlet excitons radiatively decaying and delayed microsecond or longer emission that is a consequence of the slow RISC process before fluorescence.[27,28] Recently, organic long-persistent photoluminescence (OLPL) and electroluminescence (OLEL) were reported as light generation mechanisms for compounds that have moderately large ΔE_{ST} and so are considered inefficient TADF materials.[30,31] These compounds show very long-lived emission lasting seconds after the excitation source is switched off. The long-lived luminescence originates from a charge-separation process followed by a slow charge-recombination route.[30–32] We recently demonstrated for the first time that the corresponding behavior in ECL, termed as organic long-persistent electrochemiluminescence (OLECL) also occurs in donor−acceptor (D−A) TADF compounds possessing relatively large ΔE_{ST}.[33]

The dominant design for TADF compounds relies on a twisted D−A architecture that limits the magnitude of the overlap integral of the frontier molecular orbitals, leading to a ΔE_{ST}.[34–36] A second class of TADF compounds are p/n-doped nanographenes, termed multiresonant TADF (MR-TADF) emitters, which produce the small overlap integral by exploiting complementary resonance effects of the p- and n-dopants in these polycyclic aromatic compounds.[34,37–39] Due to their rigid structure, the emission profile of MR-TADF compounds is much narrower and so the color purity is significantly enhanced. The short-range charge transfer excited state of these compounds means that the emission is only very moderately affected by solvent polarity.[39]

ECL of a series of D−A TADF emitters (2CzPN, 4CzPN, 4CzIPN, and 4CzTPN, Figure 1A) were first investigated by

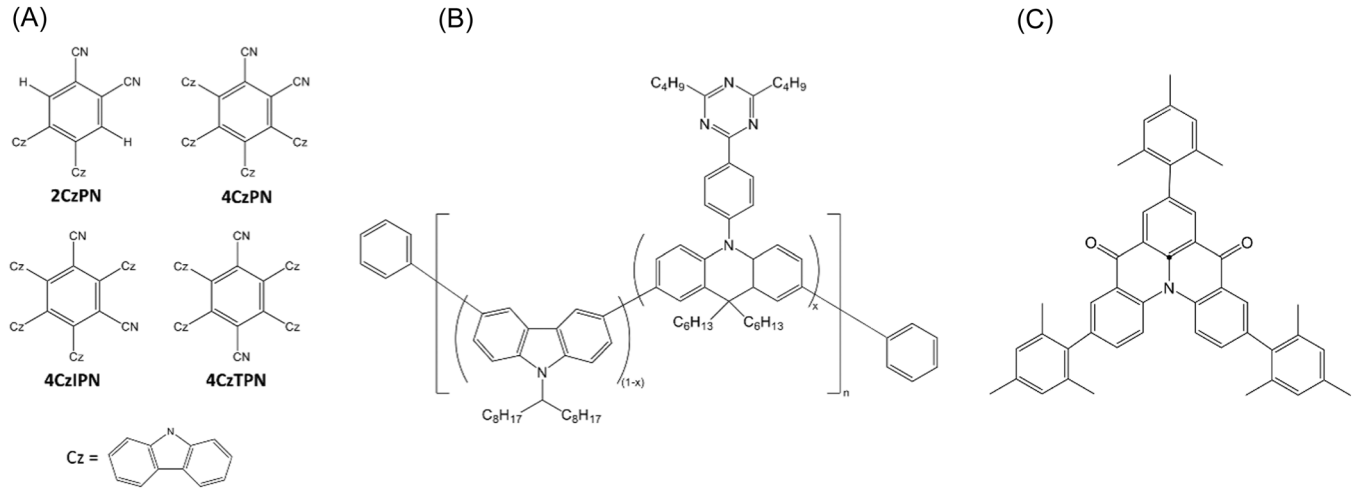

FIGURE 1 Structures of (A) 2CzPN, 4CzPN, 4CzIPN, 4CzTPN, (B) PCzAPT10 and (C) **Mes_3DiKTa**[38]

the Imato group.[40] and relative ECL efficiencies ranging from 1.1% to 47% were determined, which offers a significantly great start of such research field. Recently, The Niu group[41] reported ECL based on a TADF polymer (PCzAPT10, Figure 1B), and it was smartly applied in biosensing. The same group[42] also employed a nanoencapsulation strategy with 4CzIPN to permit ECL of this TADF emitter in an aqueous system. Despite these promising examples, research into ECL of TADF compounds is still in its infancy and insights into the interplay between TADF and ECL are required to spur the development of improved ECLphores. To date, there has been no report of the ECL behavior of MR-TADF compounds.

Herein, we report enhanced ECL of the MR-TADF molecule **Mes_3DiKTa** (Figure 1C).[38] A combination of ECL-voltage curves, ECL spectroscopy and newly designed time-resolved ECL experiments provides insight into the origin and mechanism of the ECL.

2 | EXPERIMENTAL SECTION

2.1 | Chemicals

Acetonitrile (MeCN, 99.8%), tris(2,2′-bipyridyl)ruthenium (II) hexafluorophosphate ($[Ru(bpy)_3][PF_6]_2$, 98%), tri-*n*-propylamine (TPrA, ≥98%), and ferrocene (Fc, 98%) were all obtained from Sigma-Aldrich. Tetra-*n*-butylammonium perchlorate (TBAP, electrochemical grade) as the supporting electrolyte in ECL was purchased from Alfa Aesar. Acetonitrile is anhydrous and in Sure/Seal™ bottle which is stored in a N_2 filled glove box. TPrA was stored at 4 °C in a refrigerator while all the other chemicals were stored at room temperature. **Mes_3DiKTa** was synthesized and characterized as we reported elsewhere.[38]

2.2 | Electrochemistry and ECL setup

All the electrochemistry and ECL measurements were performed in an electrochemical cell with a three-electrode system. The three-electrode system consists of a glassy carbon electrode (GCE, 3 mm in diameter) as working electrode and two platinum (Pt) wire coils as the counter and quasi-reference electrodes, respectively. The glass electrochemical cell was specially made with a flat Pyrex window at the bottom enabling the detection of generated ECL signal. During the whole experiments, the electrochemical cell was tightly sealed with a Teflon cap. An oil-resistive rubber o-ring was utilized between the cap and cell to prevent the entrance of moisture and oxygen. After each set of ECL experiments, the potential window was calibrated to the standard hydrogen electrode (SHE) potential using ferrocene/ferrocenium (Fc/Fc^+, 0.40 V vs. SHE in MeCN) as the internal standard.[43]

Cyclic voltammograms (CVs) and differential pulsed voltammograms (DPVs) were performed using a CHI 610A electrochemical analyzer (CH Instruments). All the experimental parameters including initial/final potentials, scan directions, scan rates, sweep segments and sensitivities were adjusted accordingly. A photomultiplier tube (PMT; R928) with a high voltage supply set at −750 V) was employed to detect ECL. The ECL signal as photocurrent was imported from the PMT to a source picoammeter (Keithley 6487) and transformed to a voltage signal. The PMT and CHI 610A analyzer signals were sent to a data acquisition system composed of a data acquisition board (DAQ 6036E; National Instruments) and a LabVIEW program (ECL-PMT610a.vi; National Instruments), ensuring the simultaneous measurements of electrochemistry and ECL as CVs and ECL-voltage curves. During the

experiments, the sensitivity scales on the picoammeter were set accordingly to avoid the saturation.

For the programed time-resolved ECL experiment named as time-resolved ECL observatory, an Autolab modular potentiostat (Autolab PGSTAT302N; Metrohm) with a control software NOVA was used as the ECL drive. A customer-built program pulsed the electrochemical cell with its potential limits. The interval time was setup to change the potential every 10 ms. Meanwhile, the R928 PMT connected to the source picoammeter was attached to the Autolab potentiostat via one of the two auxiliary channels. ECL signal was measured as an external signal of the Autolab and recorded at the same time with the current and applied voltage during pulsing-processes by means of NOVA software. The installation diagram of such experimental apparatus was illustrated in our previous report,[44] while much shorter potential-step duration of 10 ms was used here.

To acquire ECL spectra, the electrochemical cell containing **Mes_3DiKTa** ECL system was placed onto a spectrometer (Acton 2300i; Teledyne Princeton Instruments), which was attached with a charge-coupled device (CCD) camera (Model DU401-BR-DD-352; Andor Technology). Before spectroscopy measurement, the CCD camera was cooled down to −65 °C and the wavelength was calibrated by a mercury-argon source (Ocean Optics; HG-1). Then the accumulated spectra were recorded either with a CV scan or a potential pulsing to the **Mes_3DiKTa**/TPrA system operated using an Andor Technology program. Spooling ECL spectra were recorded with the same setup in a cyclic loop of scanning between the redox potentials that resulted in ECL.[45] Experimental parameters including the exposure time and number of kinetic series were adjusted to optimize the obtained spectra. To reduce the background interference, black curtains were positioned at the entrance to the lab, the electrochemical cell setup was covered by a black camera film exchange bag, and all the ambient light sources in the laboratory were switched off. The PL spectra were acquired by the same spectrometer-CCD camera system using a 405 nm laser (Model LDCU12/6253; Power Technology, Inc.) as the excitation light source.

2.3 | Preparations of the ECL experiments

After the electrochemical cell was thoroughly rinsed with acetone, isopropanol and ultrapure water, it was immersed in 5% KOH for 4 h and 1% HCl acid for another 4 h successively. Then the cell was cleaned with ultrapure water and dried at 120 °C in an oven. The glassy carbon working electrode was rinsed with acetone, isopropanol and ultrapure water, followed by consecutive polishing using 0.3 and 0.05 μm alumina (Al_2O_3) suspensions (Buehler Ltd.) in ultrapure water on polishing pads until a mirror-like surface was obtained. Then the working electrode was cleaned with water and dried with argon gas flow (ultrahigh purity; 99.9%; Praxair Canada Inc.). Acetone, isopropanol and ultrapure water were successively utilized again to sonicate the Pt wires as the counter and quasi-reference electrodes before a thorough clean with ultrapure water. Then the Pt wires were dried at 120 °C together with the electrochemical cell.

Before annihilation ECL experiments, the electrochemical cell and Pt coil electrodes were cooled down to room temperature. The ECL luminophore and supporting electrolyte TBAP were added to the electrochemical cell, which was moved to a N_2 filled glove box. Then the solvent acetonitrile was added to the cell inside the glove box. The cell assembly with the three-electrode system was sealed tightly and then removed from the glove box for further experiments. When the coreactant tri-*n*-propylamine (TPrA) was added to the cell, an Ar blanket was employed as a protection to prevent oxygen from entering the system.

2.4 | ECL efficiency

A relative efficiency is determined compared to the ECLphore $[Ru(bpy)_3](PF_6)_2$ by taking its efficiency as 100% under the same experimental condition using Equation (1) as below[22]:

$$\Phi_x = \frac{\left(\frac{\int_a^b \mathrm{ECL}\,dt}{\int_a^b \mathrm{Current}\,dt}\right)_x}{\left(\frac{\int_a^b \mathrm{ECL}\,dt}{\int_a^b \mathrm{Current}\,dt}\right)_{\mathrm{st}}} \times 100\% \quad (1)$$

where x represents the studied sample **Mes_3DiKTa** while st represents the standard $[Ru(bpy)_3](PF_6)_2$. The integrations of ECL intensity and current versus time indicate the photons generated and electrons injected in the system, respectively.

Furthermore, our group has recently developed new methods to determine absolute ECL efficiencies using a calibrated PMT or PMT photon counting head,[44,46] which more accurately represented the ECL performance than the relative ones:

$$\Phi_{\mathrm{ECL}} = \frac{\int \nu_{\mathrm{photon}}\,dt}{\int \nu_{\mathrm{electron}}\,dt} \times 100\% \quad (2)$$

where ν_{photon} is the total photon emission rate; and $\nu_{electron}$ is the total Faradaic electron injection rate. The former can be converted from the ECL signal detected by the PMT as the photocurrent, while the latter can be determined from the Faradaic current during the ECL process. The parameters to calculate absolute ECL efficiencies of **Mes_3DiKTa** are summarized in Supporting Information: Table S1 in the supporting information. The details of PMT calibration and calculation methods were summarized in our previous study.[44]

3 | RESULTS AND DISCUSSION

3.1 | Annihilation ECL-voltage curves

First, we investigated the electrochemical properties and ECL behavior of **Mes_3DiKTa** in the annihilation pathway. Figure 2 shows the cyclic voltammograms (CVs, gray curves) of 0.2 mmol/L **Mes_3DiKTa** in acetonitrile (MeCN) with 0.1 mol/L TBAP as the supporting electrolyte along with ECL-voltage curves (color-coded for scanning directions). In general, **Mes_3DiKTa** undergoes a quasi-reversible reduction at a peak potential of $E_{red}^{0'} = -0.93$ V where its radical anion is generated, and an oxidation at a peak potential of $E_{ox}^{0'} = 1.40$ V where its radical cation is generated, independent of the initial scanning direction. It should be noted that in our previous report, the reduction and oxidation potentials of **Mes_3DiKTa** in CVs/DPVs were located at −1.04 V (vs. SHE) and 1.78 V (vs. SHE), respectively.[38] The slight difference might arise from the difference in **Mes_3DiKTa** concentration and the different supporting electrolytes used.

Figure 2A shows the color-coded ECL-voltage curve segments corresponding to a CV in the second cycle of the potential scan starting in the cathodic direction. As the potential scan commenced at 0.00 V, the ECL signal was detected at −0.82 V (blue curve) where the radical anions were generated and reacted with the radical cations that were already within the diffusion layer. The onset ECL potential at −0.82 V matches well with the electrochemical current onset potential in CVs. Interestingly, during the ECL devolution process, upon reversing the potential scan direction to anodic (red segment in Figure 2A), the ECL signal did not decrease to 0 immediately. Instead, it decreased very slowly until the potential reached around 1.00 V, showing an unexpectedly long ECL decay that has scarcely been observed in the ECL literature involving TADF emitters. In the anodic ECL process, the onset-ECL potential is located at 1.18 V (red segment in Figure 2A), corresponding well to the oxidation onset potential recorded in the CV. After

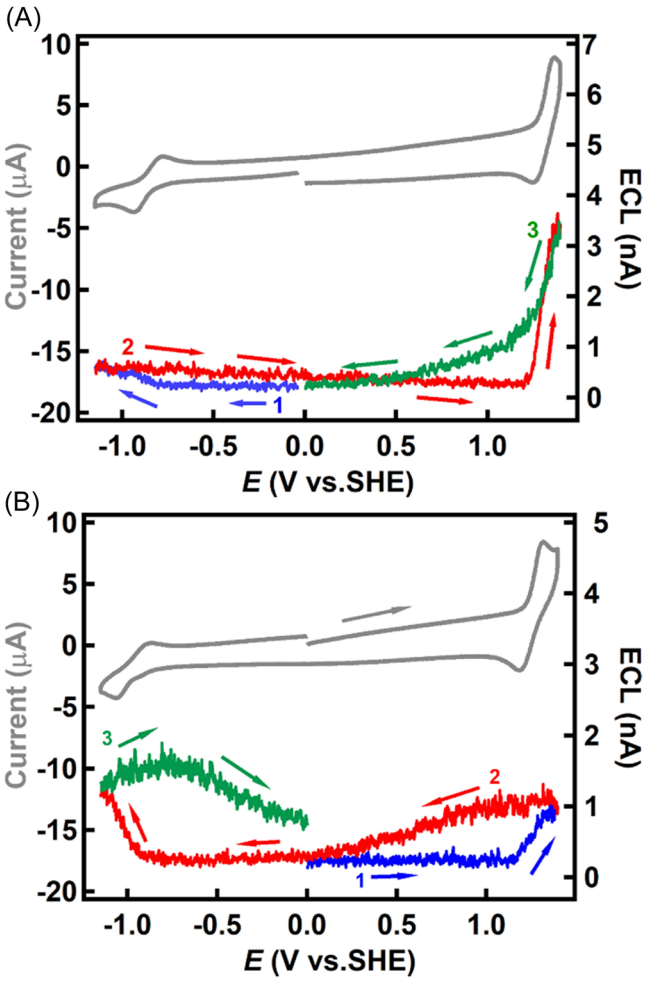

FIGURE 2 Cyclic voltammogram (CVs, gray) and ECL-voltage curves (color-coded) of 0.2 mmol/L **Mes_3DiKTa** in MeCN at a scan rate of 0.1 V/s with 0.1 mol/L TBAP as the supporting electrolyte with (A) negative scan initially and (B) positive scan initially. ECL, Electrochemiluminescence; TRAP, Tetra-*n*-butylammonium perchlorate.

reaching a peak intensity of 3 nA, the ECL signal gradually devolved, slowly decreasing to 0 nA at around 0.3 V (green segment in Figure 2A), demonstrating again a long ECL emission decay. When the initial potential scan direction is changed to anodic (Figure 2B), both the anodic (red segment) and cathodic (green segment) ECL show a slow devolution as well; however, the maximum ECL intensity is somewhat attenuated in this experiment and does depend on the initial scan direction: The lower maximum ECL of 2 nA indicates that the radical anion is more persistent than the radical cation of **Mes_3DiKTa**, which is aligned with the more reversible reduction process observed in the CV.

We then expanded the potential window of the CV of **Mes_3DiKTa** to explore how the ECL would evolve. In Supporting Information: Figure S1, the CV (gray) displays

second reduction and second oxidation waves at peak potentials of −1.18 V and 1.70 V, respectively. The redox behavior is better revealed in the differential pulsed voltammograms (DPVs, Supporting Information: Figure S2). An extra ECL peak can be observed in both the cathodic (blue segment) and anodic (orange segment) potential regions. Both these ECL peaks are enhanced, probably by the presence of a greater concentration of radical cations and anions that are produced via the reaction between dications/dianions and neutral **Mes$_3$-DiKTa** (Supporting Information: Scheme S1). The long ECL emission decay in the devolution processes for the two extra ECL waves can also be observed. When [Ru(bpy)$_3$](PF$_6$)$_2$ was used as a reference (Supporting Information: Figure S3) under the same experimental condition, the relative ECL efficiency of **Mes$_3$DiKTa** in Figure 2A was calculated to be 94% while its efficiency upon extended scanning, as in Supporting Information: Figure S1, was determined to be 118%, both of which are superior to most other reported organic molecules. ECL efficiencies of organic molecules reported in recent years have been summarized in our previous report[43] (before 2018) as well as in Supporting Information: Table S2 (2019–now). The annihilation ECL can be further enhanced by applying a pulsed-potential method at 10 Hz (Supporting Information: Figure S4); under these conditions the relative ECL efficiency was determined to be 136%. Moreover, the absolute ECL efficiencies of **Mes$_3$DiKTa** were determined to be 0.0013% in expanded CVs scans and 0.66% with 10 Hz pulsing, respectively. Again, **Mes$_3$DiKTa** demonstrates an unusually long ECL emission decay, and a much higher ECL efficiency than most of the previously reported organic compounds used as ECLphores, whatever the potential window or the scan direction that is used.

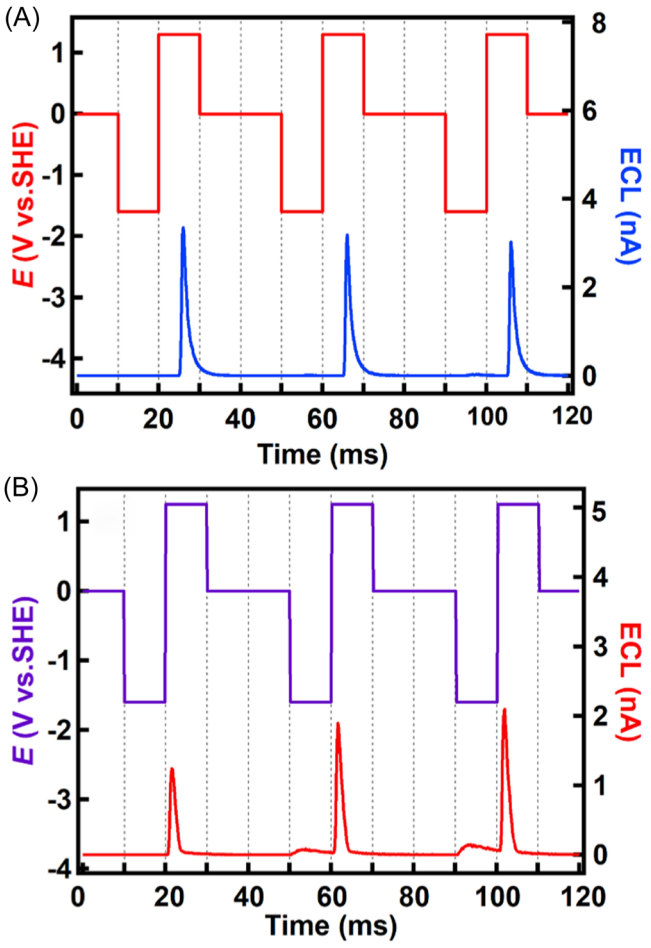

FIGURE 3 Time-resolved ECL curves with ECL-time observatory experiments of 0.2 mmol/L **Mes$_3$DiKTa** (A) and 0.2 mmol/L [Ru(bpy)$_3$](PF$_6$)$_2$ (B) in acetonitrile via annihilation pathway. ECL, electrochemiluminescence.

3.2 | Annihilation ECL-time observatory

To investigate the slow ECL devolution process and the long ECL emission decay, we then designed an ECL platform to reveal the time-resolved ECL behavior based on programmed potential pulsing experiments. Figure 3A demonstrates three cycles of time-resolved ECL curves of **Mes$_3$DiKTa** (blue) with the potential applied (red). There are four steps in each cycle. With the first cycle as an example, in step one, the applied potential was set at 0 V for 10 ms with no ECL observed (blue curve in Figure 3A). In the second step the potential was changed to −1.7 V for another 10 ms, the radical anion of **Mes$_3$DiKTa** was generated and no ECL signal was seen within this range since there are no radical cations produced yet. In step three when the potential was applied at 1.2 V for 10 ms, an enhancement of the ECL (around 3 nA) was observed. Interestingly, the ECL was not induced immediately when the potential was stepped to 1.2 V but instead the onset ECL was delayed by about 5 ms from the moment of potential switching. After the ECL reached a maximum, the ECL decayed gradually, lasting ~10 ms, even after the potential was brought back to 0 V in step four. The decay process in step three can be seen more clearly in Supporting Information: Figure S5 when the observed ECL intensity is presented on a logarithmic scale. The applied potential is kept 0 V in the last step for 10 ms and the ECL signal decays to 0 within this time window. As such, a ~5 ms delay of the onset of the ECL and ~10 ms associated with the ECL decay were observed in the ECL evolution and ECL devolution processes of **Mes$_3$DiKTa**, respectively. The ~10 ms ECL emission decay matches well with the observation in the ECL-voltage curves.

The potential-pulsing experiment described above documents both a delayed onset of the ECL and a long ECL emission decay process. Instead of conventional potential pulsing between the first oxidation and reduction potentials, our time-resolved ECL platform provides greater sensitivity to observe such phenomena. The time-resolved ECL platform is simple to construct and easy to adjust.

The unexpected delay of the onset-ECL and long ECL decay might originate from one/some of the following mechanisms, which have been used to explain photoluminescence (PL) phenomena: (1) phosphorescence, (2) TTA, (3) TADF and (4) OLPL. In addition, the Marcaccio group[47] reported ECL of a series of sulfurated pyrene-cored dendrimer and found delayed ECL onset from 7 ms to 13 ms depending on the molecular size. The authors attributed the delay to a combination of two factors: the decrease in the electron-transfer constant and the decrease of the diffusion coefficient as a consequence of the molecular size increase. However, such conclusion does not apply to **Mes_3DiKTa** due to its different molecular sizes from the dendrimers. Furthermore, slow diffusion of the radical ions, and uncompensated solution resistance in the experiment may contribute to the delay in the onset-ECL.[48] For comparison, we performed the exact same time-resolved ECL experiments for the well-studied $[Ru(bpy)_3](PF_6)_2$ (Figure 3B). Three cycles are shown with the potential pulsed from zero to oxidation, reduction and back to zero. For this compound the ECL signal (red curve) emerges and decays immediately following the generation of the radicals (purple curve). No delayed onset ECL and much shorter ECL emission decay for $[Ru(bpy)_3](PF_6)_2$ are observed. Since $[Ru(bpy)_3](PF_6)_2$ is a phosphorescent ECLphore[49] and the experiment was performed using the same condition as **Mes_3DiKTa**, it is reasonable to rule out phosphorescence and slow diffusion as an explanation for the observed kinetics. It should be noted that in the time-resolved ECL experiments for both **Mes_3DiKTa** and $[Ru(bpy)_3](PF_6)_2$, in the first cycles there is no ECL when a negative potential was applied (step two), but small ECL bumps are observed under negative potentials in the second and third cycles. This is because that in the second and third cycles, radical cations have been produced at positive potentials to generate ECL with radical anions that were formed at negative potentials. In the first cycle, however, the positive potential has not been applied yet and no radical cations are existing in the diffusion layer resulting no ECL in step two.

We then performed the time-resolved ECL experiments under the same experimental conditions with 9,10-diphenylanthracene (DPA), a molecule that exhibits TTA[50] and a delayed ECL due to uncompensated solution resistance.[48] The results are shown in Supporting Information: Figure S6A. Taking the first cycle as an example, in step three when the radical cations are generated and interact with the radical anions, the onset ECL (red) was delayed by ~0.5 ms after the potential was switched (blue curve). This delay can be seen more clearly in Supporting Information: Figure S6B. After reaching the peak value, the ECL then decayed to zero even after the potential was changed back to 0 in step four. Based on the similarity in ECL behavior between DPA and **Mes_3DiKTa**, it is plausible to assign TTA and/or uncompensated solution resistance as an operational light generation mechanism for both compounds and one that is responsible for the onset-ECL delay (Equation (3) and Equation (4), note that the energy between triplet excitons is sufficient to produce compounds in higher lying singlet excitons, these would rapidly relax through internal conversion to generate ^1R).

$$^3R + {}^3R \rightarrow {}^nR^* + R \tag{3}$$

$$^nR \rightarrow {}^1R^*$$

$$^1R^* \rightarrow R + h\nu \tag{4}$$

For **Mes_3DiKTa**, given the concentrations used in the ECL experiment, after triplet excitons are electrochemically generated, both monomolecular upconversion of triplet excitons to singlets by RISC (green, TADF), and bimolecular interaction of two triplet excitons to form a singlet and a compound in its ground state via TTA (blue) are possible, as illustrated in Scheme 1. The delayed onset of the ECL may arise in part from the time require for the two triplet excitons to diffuse and recombine. The long ECL decay, however, cannot be explained only by photophysical phenomena as the delayed lifetimes of TTA and TADF materials are normally in the microsecond regime.

Notably, the delayed onset-ECL of DPA was only ~0.5 ms, which is one order of magnitude faster than that observed for **Mes_3DiKTa** at 5 ms. Thus, TTA/TADF, and/or uncompensated solution resistance cannot solely account for the unusually long delay in the onset of the ECL. OLPL proceeds on a timescale similar to what we have observed here for the ECL. We contend that a similar process, OLECL, could also be operational for **Mes_3DiKTa**, a behavior similar to a family of inefficient D−A TADF compounds that we recently documented.[33] In many of the OLPL and OLEL reports, charge separation and slow charge recombination occur from exciton aggregates (exciplex).[31,32] For our ECL, the investigation of emission from exciton aggregates significantly depends on the ECL spectroscopy (*vide infra*.).

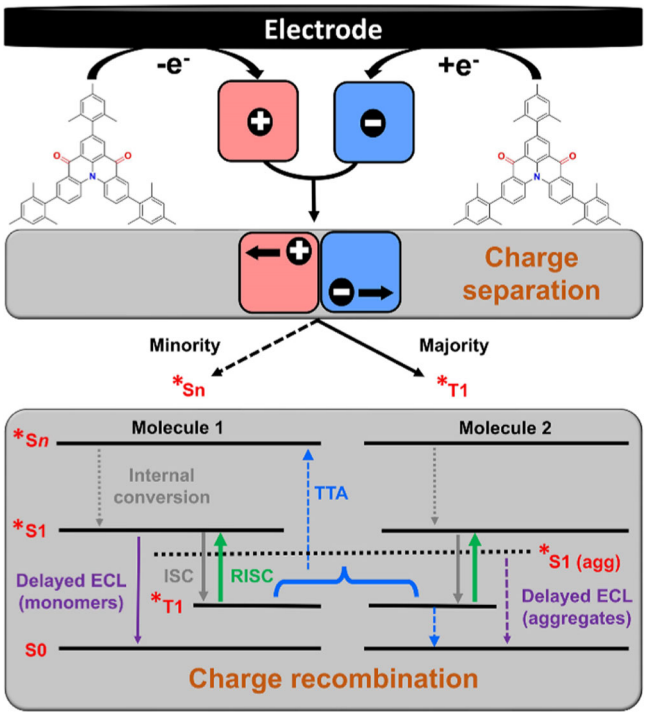

SCHEME 1 Qualitative diagram of the excitons' behaviors including TTA, TADF and OLECL. OLECL, organic long-persistent electrochemiluminescence; TADF, thermally activated delayed fluorescence; TTA, triplet-triplet annihilation.

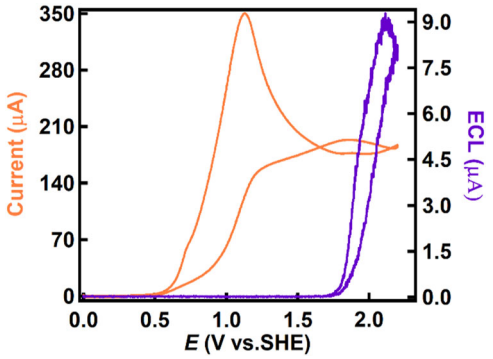

FIGURE 4 Cyclic voltammogram (CVs, orange) and ECL-voltage curve (purple) of 0.2 mmol/L **Mes_3DiKTa** with 20 mmol/L TPrA as the co-reactant in acetonitrile at a scan rate of 0.1 V/s with 0.1 mol/L TPAP as the supporting electrolyte. ECL, electrochemiluminescence.

3.3 | Coreactant ECL

We next investigated the ECL behavior under co-reactant conditions, using TPrA radicals as a sacrificial reductant, which are formed after electrooxidation and deprotonation of the radical cation. In the presence of 20 mmol/L TPrA, the ECL intensity of **Mes_3DiKTa** in a cyclic potential scanning between 0.00 and 2.20 V was greatly enhanced to ~9 μA (Figure 4). The ECL efficiency was determined to be 79% relative to the $[Ru(bpy)_3](PF_6)_2$/TPrA coreactant system (Supporting Information: Figure S7) while the absolute efficiency was calculated to be 1.1%, both of which are significantly higher compared to most other organic compounds (Supporting Information: Table S2). The ECL onset potential is located at around 1.42 V, which is close to the first oxidation potential (1.40 V). During the ECL devolution, the ECL intensity decreased slowly as the potential was scanned cathodically back to 0.00 V. It is worth noting that the devolution curve essentially parallels the evolution one. As in the annihilation ECL experiments, there is a very long ECL emission decay for **Mes_3DiKTa**. As well, similar to annihilation ECL experiments, the ECL signal is enhanced when a traditional pulsed-potential method at 10 Hz was applied as seen in Supporting Information: Figure S8. Here, the relative ECL efficiency is 56% while the absolute efficiency is 1.5%. It should be noted that compared with those during potentiodynamic scans (Figure 4), the relative ECL efficiency is lower (56% vs. 79%) while absolute ECL efficiency is higher (1.5% vs. 1.1%) during potential pulsing. Such a difference can be ascribed by the unavoidable error during the relative ECL efficiency measurement; the differences in radical behavior (radical stability and radical reactivity) between $[Ru(bpy)_3](PF_6)_2$ and **Mes_3DiKTa** were not considered.

Our time-resolved ECL experiments were performed again with the **Mes_3DiKTa**/TPrA coreactant system. Three cycles of time-resolved ECL (blue) with the potential being pulsed from 0 to 2.1 V and back to 0 V in 10 ms steps (orange) are shown in Figure 5A. The observation time period at the end of each cycle was set to 10 ms to detect the delayed ECL of **Mes_3DiKTa**. The applied potential was set to 0 V initially and no ECL signal was observed. When the potential was stepped to 2.1 V for 10 ms, no ECL was detected for the first ~5 ms; however, there was a progressive increase in ECL intensity after this point. The ECL intensity did not decay to 0 from the peak value immediately after the voltage step returned to 0 V but lasted for ~1 ms. The decay process is revealed in greater detail in Supporting Information: Figure S9. It is plausible that the 5 ms delayed onset-ECL and the 1 ms extra ECL emission decay are attributed to slow diffusion and recombination of polarons (i.e., radical cations and anions) before emission proceeding by TTA and/or the OLECL processes. For comparison, the time-resolved ECL experiments were performed with the $[Ru(bpy)_3](PF_6)_2$/TPrA co-reactant system. As shown in Figure 5B, FOR each cycle the potential was stepped from 0 to 2.1 V and back to 0 V with a step and observation time each of 10 ms. The ECL signal appeared only when a potential of 2.1 V was applied to the oxidation limit while no ECL was

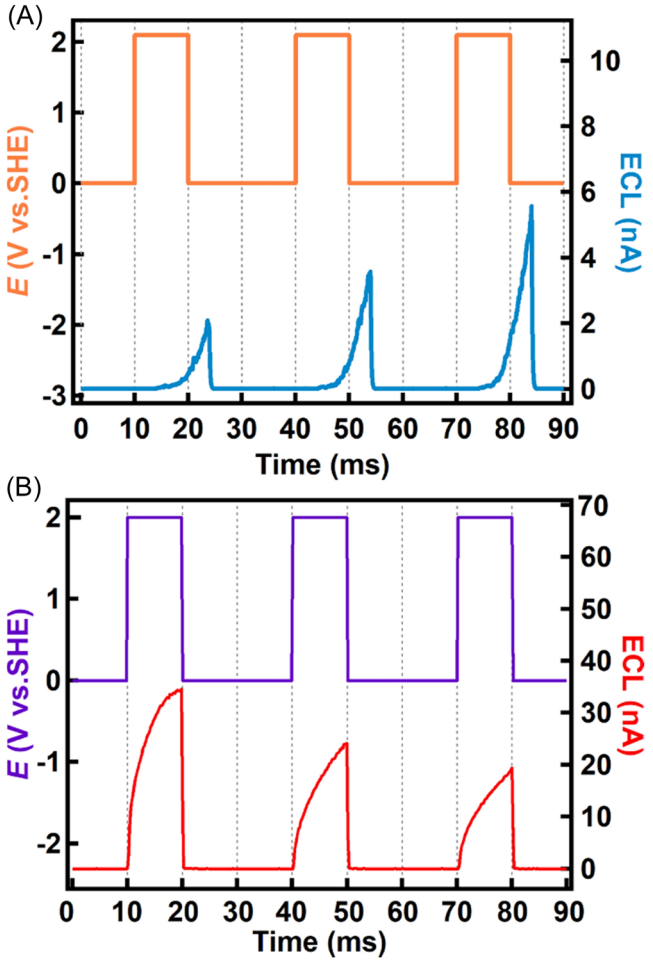

FIGURE 5 Time-resolved ECL curves with ECL-time observatory experiments of 0.2 mmol/L (A) **Mes_3DiKTa** and (B) $[Ru(bpy)_3](PF_6)_2$ in acetonitrile via TPrA coreactant pathway.

observed when the potential stepped to 0 V. The ECL evolution and devolution followed the potential steps while both the ECL delay and overshot were negligible. In other words, the ECL arises and vanishes spontaneously with the steps of the applied potential for this compound. This contrasting observation once again provides strong evidence of an emission generation mechanism in the ECL that is distinct from that observed under photoluminescence conditions.

3.4 | ECL spectroscopy

Next, the annihilation and co-reactant ECL spectra were acquired, respectively, and compared with the PL spectrum as shown in Figure 6. The peak wavelength of PL (blue) is located at 478 nm while the annihilation (red) and coreactant (green) ECL spectra possess the same peak wavelength at 498 nm, both of which are red shifted (20 nm) compared with the PL spectrum. Since all the

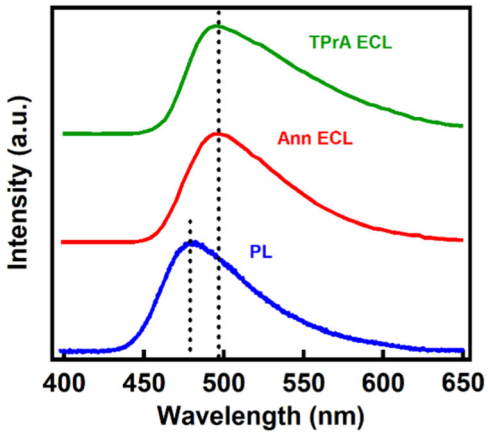

FIGURE 6 ECL spectra of **Mes_3DiKTa** via annihilation pathway (red), TPrA coreactant pathway (green), and PL spectrum of **Mes_3DiKTa** (excited at 405 nm, blue). ECL, electrochemiluminescence; PL, photoluminescence.

three spectra were acquired using the identical solution with the same spectrometer and CCD camera, it may be ruled out that the 20 nm red shift of the ECL compared to the PL is from self-absorption (or inner filter effect) due to the concentration difference between PL and ECL systems. Instead, it must originate at least in part from new species generation during ECL, such as ECL from an aggregate. Mechanistically, this would imply that when potentials were applied to the system, a charge-transfer (CT) state would be generated within the aggregate. The CT state could then become a charge-separated state that consists of a radical cation and radical anion followed by the recombination of the radical ions to generate the aggregate excitons. ECL would then occur upon the relaxation of the aggregate excitons, which typically have a smaller HOMO−LUMO gap,[51] displaying a red shifted PL compared with the PL from the monomer excitons. This observed behavior, especially the slow charge recombination process, led to our assignment that the ECL emission results from OLECL to explain the delayed onset-ECL and the long ECL emission decay.

For the **Mes_3DiKTa** ECL system, it should be noted that the emission from the aggregate might be distinct and distinguishable between annihilation and coreactant pathways. During the annihilation ECL process, there are no other chromophoric species in the solution to interact with **Mes_3DiKTa**. As a result, the intermolecular interaction most likely occurred between **Mes_3DiKTa** radicals, which then formed a bound exciton-ground state aggregate (analogous to excimer). During the coreactant ECL, two plausible mechanisms must be considered based on the coreactant ECL mechanisms with TPrA, as summarized by Miao.[2] On the one hand, after the deprotonation of TPrA radical

cation ($TPrA^{\cdot+}$), the TPrA radical ($TPrA^{\cdot}$) could reduce the **Mes_3DiKTa** radical cation to generate the **Mes_3DiKTa** exciton. In this first case, since there is no **Mes_3DiKTa** radical anion produced, an aggregate (analogous to exciplex) consisting of a **Mes_3DiKTa** radical cation and a NEt_3^+ could possibly lead to the OLECL. On the other hand, the $TPrA^{\cdot}$ could also reduce a neutral **Mes_3DiKTa** molecule to form an **Mes_3DiKTa** radical anion, which could interact with **Mes_3DiKTa** radical cation in a similar way to an annihilation ECL route. In this second mechanism, the system contains **Mes_3DiKTa** radical cations, **Mes_3DiKTa** radical anions and NEt_3^+ species. Both aggregates of **Mes_3DiKTa** radicals and aggregates of **Mes_3DiKTa**/NEt_3^+ may exist. In fact, when we normalized and overlapped the annihilation and co-reactant ECL spectra in Supporting Information: Figure S10, a small difference could be observed that can be attributed to the fact that only aggregates of **Mes_3DiKTa** radicals were generated in the annihilation ECL process, while both excimer-like aggregates of **Mes_3DiKTa** radicals, and exciplex-like aggregates of **Mes_3DiKTa**/NEt_3^+ were produced within co-reactant ECL pathway with TPrA. It should be noted that in the ECL spectra, a shoulder at around 478 nm was also observed, corresponding to the monomer emission, based on the comparison with the PL spectrum (Figure 6). As such, it is plausible that ECL emission comes from a combination of exciton monomers and exciton aggregates, the latter of which leads to its OLECL behaviors. Such comprehensive ECL processes including OLECL, TTA and TADF are illustrated in Scheme 1.

Emissions in both ECL and PL occur from the singlet excited state as triplet excitons would either be converted to singlet excitons by RISC at ambient temperature due to the small ΔE_{ST} (0.19 eV in toluene)[38] or recombine via TTA. Direct phosphorescence is unlikely to occur as this is a formally spin-forbidden process and there is little spin-orbit coupling to turn on this radiative decay mode, further the recorded phosphorescence peak of **Mes_3DiKTa** is at 514 nm, at higher energy than the recorded maximum of the ECL, and phosphorescence was not previously observed at ambient temperature during photoexcitation of the compound in toluene solution. To efficiently generate the excited state, the enthalpy of ECL generation reactions determined from the peak potentials of the redox waves should be greater than that of the excitons determined from the emission peak wavelength[52]:

$$E_p(R'/R'^{\bullet+}) - E_p(R/R^{\bullet-}) - 0.16(eV) \geq -\Delta H^o \quad (5)$$

where $E_p(R'/R'^{\bullet+})$ and $E_p(R/R^{\bullet-})$ are the oxidation and reduction peak potentials, respectively, obtained from CVs; $-\Delta H^o$ represents the enthalpy of fluorescence and/or phosphorescence (although not detected in our experiments) of the excitons. Note that in an ECL process, triplets excitons are more dominant rather than singlet excitons thermodynamically, which is because the enthalpy of triplet (longer wavelength) is smaller than that of singlet excitons (shorter wavelength).[53]

For the annihilation ECL process, the enthalpy for the annihilation reaction (2.22 eV, from CVs) is inferior to that of singlet (2.49 eV, calculated from Figure 6), while being very close to that of triplet excitons (2.27 eV, calculated from our previous report[38]). This result indicates that the system energy to produce singlet excitons is insufficient, while the energy to generate triplet excitons is marginal. For the coreactant ECL with TPrA, thermodynamically, the enthalpy of the coreactant reaction to generate the excitons was determined to be 2.94 eV from the difference between the **Mes_3DiKTa** oxidation potential (1.40 V) and the reduction potential of TPrA radical that is −1.70 V[17] using Equation (5). The reaction enthalpy is sufficiently large to populate both singlet (2.49 eV) and triplet (2.27 eV) excitons directly, and singlet states can be produced via RISC and/or TTA from triplet states thereafter.

Compared to our recent report on a series of 2CzPN \TADF derivatives[33] showing OLECL in annihilation pathway, **Mes_3DiKTa** displayed the delayed ECL onset and long ECL decay not only in annihilation but also in co-reactant ECL routes with TPrA. Furthermore, the ECL efficiencies of **Mes_3DiKTa** are significantly higher than the reported D−A TADF compounds although the existence of **Mes_3DiKTa** aggregates have also been demonstrated in the ECL processes. The ECL data of such D−A TADF series and MR-TADF molecule **Mes_3DiKTa** was summarized in Supporting Information: Table S3.

Figure 7 shows a representative example of the spooling ECL spectra[45] of 0.2 mmol/L **Mes_3DiKTa** in the presence of 20 mmol/L TPrA with a potential scanning cycle from 0 to 1.80 V and then back to 0 V. The spectra provide further insight into the ECL mechanism. The ECL spectra are color-coded in gray, red and blue. When the potential is scanned to 1.42 V, which is close to the first oxidation peak of **Mes_3DiKTa** (Supporting Information: Figure S1), **Mes_3DiKTa** is oxidized to its radical cation. At the same time, the strongly reducing species $TPrA^{\cdot}$ is generated through TPrA oxidation ($E_{ox} = 0.83$ V) and subsequent deprotonation. This latter species reduce the radical cations of **Mes_3DiKTa** to form **Mes_3DiKTa*** (as well its aggregates) that are responsible for the ECL (Supporting Information: Scheme S2). The ECL intensity increased from 0 at 1.42 V (red curves), which corresponds to the

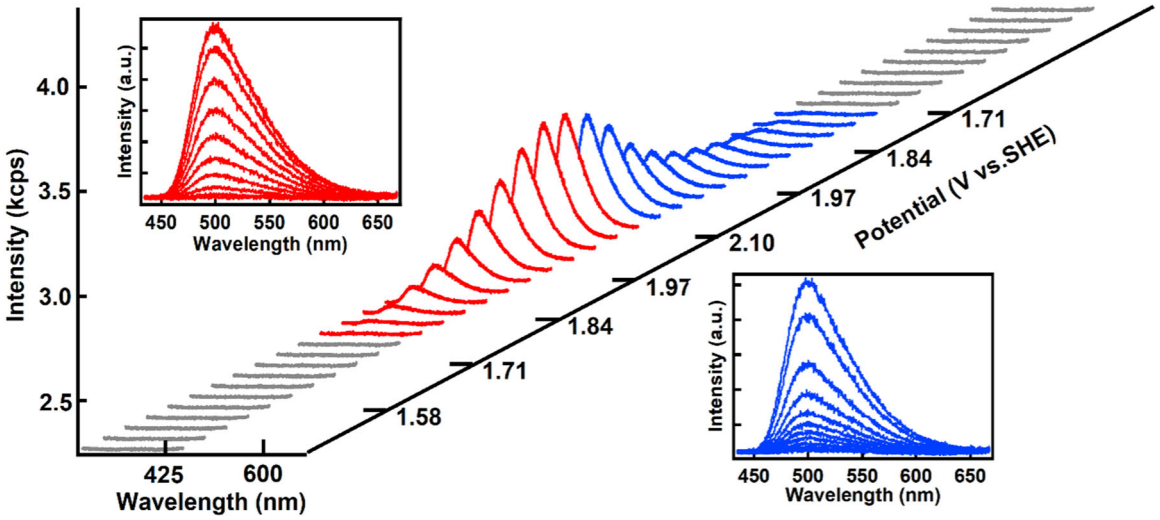

FIGURE 7 Spooling ECL spectra 0.2 mmol/L **Mes_3DiKTa** in the presence of 20 mmol/L TPrA, with a scan rate of 0.02 V/s and exposure time of 2 s. ECL, electrochemiluminescence.

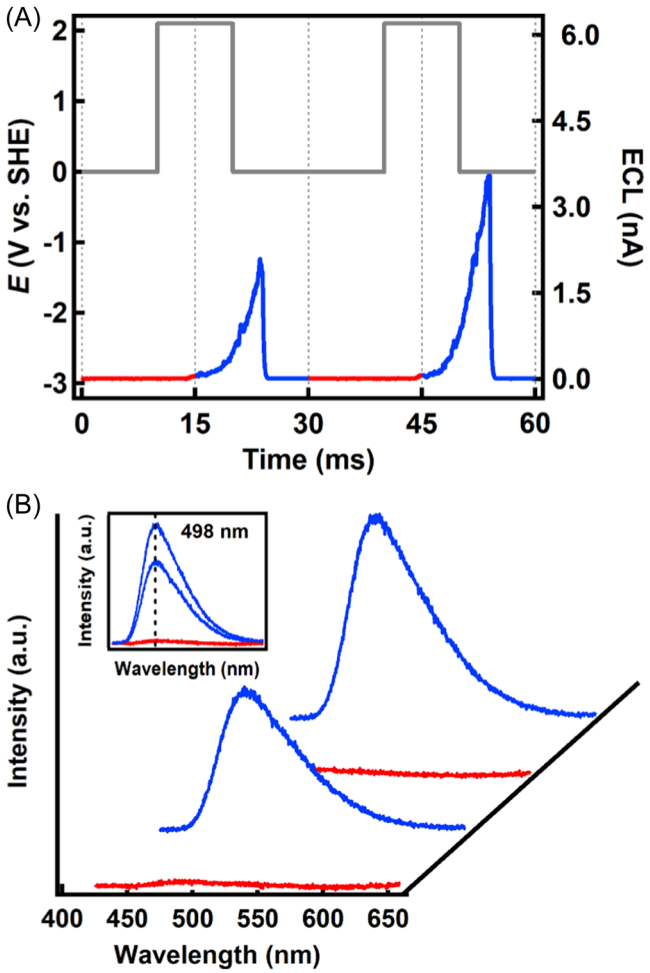

FIGURE 8 (A) Time-resolved ECL curves with ECL-time observatory experiments of 0.2 mmol/L **Mes_3DiKTa**. (B) Spooling ECL spectra obtained spontaneously. The red and blue parts in Figure 8B corresponds to the red and blue parts in Figure 8A, respectively. ECL, electrochemiluminescence.

onset ECL potential in Figure 4, and reaches a maximum value at 1.8 V. With the reverse scan, the spectra decrease progressively to 0 at 1.42 V (blue curves). Within each of the spectra, the ECL retain the same shape and peak wavelength (Figure 7, inset), indicating the same excitons are present throughout the whole process.

Our time-resolved ECL experiments and ECL spectroscopy were then combined to investigate the putative OLECL behavior. Figure 8A displays two cycles of 10 ms potential steps. Since there is a 5 ms delay for ECL generation, the spectrograph and CCD camera were set purposely to take an ECL spectrum every 15 ms (Figure 8A). In the first cycle, the weak ECL part (red-coded) in Figure 8A generates a low-intensity spectrum (red) in Figure 8B while a more intense ECL signal (blue-coded) in Figure 8A produces a more intense spectrum in Figure 8B. Both the weak and the intense ECL possess the same peak maxima (c.f. the inset in Figure 8B), indicating the same excitons are generated over the entire process. These observations are reproducible over 20 cycles. These results reveal for the first time the ECL of an MR-TADF compound and demonstrate a second instance of OLECL behavior.

4 | CONCLUSION

Here, we report the ECL properties of an MR-TADF compound for the first time. We observed enhanced ECL for **Mes_3DiKTa** by means of ECL-voltage curves, ECL-time curves in newly designed observatory and ECL spectroscopy. We attribute the unusual ECL behavior to an OLECL mechanism that we contend is possible in

TADF systems with moderate ΔE_{ST}; TTA/TADF cannot be ruled out as contributing to the ECL signal given the concentration of emitter used in the ECL experiments. As a result, relative ECL efficiency of **Mes_3DiKTa** was determined to be 118% and 79% to $[Ru(bpy)_3](PF_6)_2$ under annihilation and co-reactant conditions, respectively, and absolute ECL efficiencies were calculated to be 0.0013% in annihilation and 1.1% with coreactant, which are some of the highest reported among all the organic ECL materials. Our investigation using the newly designed time-resolved ECL experiments has demonstrated a delay time for the onset of the ECL of 5 ms in both annihilation ECL and coreactant ECL routes, which we contend arises from the contribution of OLECL. ECL spectroscopy provides evidence of a combination of monomer and aggregates (analogous to excimer in annihilation route, and to exciplex in coreactant pathway, respectively) emissions. The OLECL leads to an ECL enhancement with higher quantum efficiency. The delayed ECL onset and long ECL emission decay process could be potentially exploited in ECL sensing/imaging.

ACKNOWLEDGMENTS

We appreciate very much the financial supports to this study by Natural Sciences and Engineering Research Council Canada (NSERC, DG RGPIN-2018-06556 and SPG STPGP-2016-493924), Canada Foundation of Innovation/Ontario Innovation Trust (CFI/OIT, 9040) and The University of Western Ontario. We are grateful to the quality service from our Electronic Shop in Chemistry, Glass Shop and ChemBioStores. L. D. is grateful to the financial support from Guangxi province, China for her visiting professorship in Canada. The St Andrews team would also like to thank the Leverhulme Trust (No. RPG-2016047) and EPSRC (No. EP/P010482/1) for financial support. EZ-C is a Royal Society Leverhulme Trust Senior Research Fellow (No. SRF\R1\201089). Computational resources have been provided by the Consortium des Équipements de Calcul Intensif (CÉCI), funded by the Fonds de la Recherche Scientifiques de Belgique (F. R. S.-FNRS) under Grant No. 2.5020.11, as well as the Tier-1 supercomputer of the Fédération Wallonie-Bruxelles, infrastructure funded by the Walloon Region under the grant agreement n1117545. Y.O. acknowledges funding by the Fonds de la Recherche Scientifique-FNRS under Grant n° F.4534.21 (MIS-IMAGINE).

CONFLICT OF INTEREST

The authors declare no conflict of interest.

DATA AVAILABILITY STATEMENT

The data that support the findings of this study are available in the supplementary material of this article.

ORCID

Yoann Olivier https://orcid.org/0000-0003-2193-1536
Eli Zysman-Colman https://orcid.org/0000-0001-7183-6022
Zhifeng Ding https://orcid.org/0000-0001-9252-9320

REFERENCES

1. Hesari M, Ding Z. Review-electrogenerated chemiluminescence: light years ahead. *J Electrochem Soc*. 2015;163(4):H3116-H3131.
2. Miao WJ. Electrogenerated chemiluminescence and its biorelated applications. *Chem Rev*. 2008;108(7):2506-2553.
3. Liu Z, Qi W, Xu G. Recent advances in electrochemiluminescence. *Chem Soc Rev*. 2015;44(10):3117-3142.
4. Zhu H, Jiang D, Zhu J-J. High-resolution imaging of catalytic activity of a single graphene sheet using electrochemiluminescence microscopy. *Chem Sci*. 2021;12(13):4794-4799.
5. Li L, Chen Y, Zhu J-J. Recent advances in electrochemiluminescence analysis. *Anal Chem*. 2017;89(1):358-371.
6. Wang N, Gao H, Li Y, et al. Dual intramolecular electron transfer for in situ coreactant-embedded electrochemiluminescence microimaging of membrane protein. *Angew Chem Int Ed*. 2021;60(1):197-201.
7. Huang Z, Li Z, Xu L, et al. Mechanistic insight into a novel ultrasensitive nicotine assay base on high-efficiency quenching of gold nanocluster cathodic electrochemiluminescence. *Anal Chem*. 2020;92(16):11438-11443.
8. Wang Z, Pan J, Li Q, et al. Improved AIE-active probe with high sensitivity for accurate uranyl ion monitoring in the wild using portable electrochemiluminescence system for environmental applications. *Adv Funct Mater*. 2020;30(30):2000220.
9. Jiang X, Wang H, Chai Y, Shi W, Yuan R. High-efficiency CNNS@NH_2-MIL(Fe) electrochemiluminescence emitters coupled with Ti_3C_2 nanosheets as a matrix for a highly sensitive cardiac troponin I assay. *Anal Chem*. 2020;92(13):8992-9000.
10. Voci S, Duwald R, Grass S, et al. Self-enhanced multicolor electrochemiluminescence by competitive electron-transfer processes. *Chem Sci*. 2020;11(17):4508-4515.
11. Wang Y, Zhao G, Chi H, et al. Self-luminescent lanthanide metal–organic frameworks as signal probes in electrochemiluminescence immunoassay. *J Am Chem Soc*. 2021;143(1):504-512.
12. Wong JM, Zhang R, Xie P, et al. Revealing crystallization-induced blue-shift emission of a di-boron complex by enhanced photoluminescence and electrochemiluminescence. *Angew Chem Int Ed*. 2020;59(40):17461-17466.
13. Yang L, Hendsbee AD, Xue Q, et al. Atomic precision graphene model compound for bright electrochemiluminescence and organic light-emitting diodes. *ACS Appl Mater Interfaces*. 2020;12(46):51736-51743.
14. Yang L, Koo D, Wu J, et al. Benzosiloles with crystallization-induced emission enhancement of electrochemiluminescence: synthesis, electrochemistry, and crystallography. *Chem Eur J*. 2020;26(51):11715-11721.
15. Chu K, Adsetts JR, He S, et al. Electrogenerated chemiluminescence and electroluminescence of N-doped graphene quantum dots fabricated from an electrochemical exfoliation process in nitrogen-containing electrolytes. *Chem Eur J*. 2020;26(68):15892-15900.
16. Hesari M, Ding Z. A grand avenue to Au nanocluster electrochemiluminescence. *Acc Chem Res*. 2017;50(2):218-230.

17. Hesari M, Workentin MS, Ding Z. Highly efficient electrogenerated chemiluminescence of Au38 nanoclusters. *ACS Nano*. 2014;8(8):8543-8553.
18. Zhang RZ, Adsetts JR, Nie YT, Sun XH, Ding ZF. Electrochemiluminescence of nitrogen- and sulfur-doped graphene quantum dots. *Carbon*. 2018;129:45-53.
19. Qin Y, Wang Z, Xu J, et al. Carbon nitride quantum dots enhancing the anodic electrochemiluminescence of ruthenium(II) tris(2,2′-bipyridyl) via inhibiting the oxygen evolution reaction. *Anal Chem*. 2020;92(23):15352-15360.
20. Rudmann H, Shimada S, Rubner MF. Solid-state light-emitting devices based on the tris-chelated ruthenium(II) complex. 4. High-efficiency light-emitting devices based on derivatives of the tris(2,2'-bipyridyl) ruthenium(II) complex. *J Am Chem Soc*. 2002;124(17):4918-4921.
21. Tokel-Takvoryan NE, Hemingway RE, Bard AJ. Electrogenerated chemiluminescence. XIII. Electrochemical and electrogenerated chemiluminescence studies of ruthenium chelates. *J Am Chem Soc*. 1973;95(20):6582-6589.
22. Wallace WL, Bard AJ. Electrogenerated chemiluminescence. 35. Temperature dependence of the ECL efficiency of tris(2,2'-bipyridine)rubidium(2+) in acetonitrile and evidence for very high excited state yields from electron transfer reactions. *J Phys Chem*. 1979;83(10):1350-1357.
23. Fabrizio EF, Prieto I, Bard AJ. Hydrocarbon cation radical formation by reduction of peroxydisulfate. *J Am Chem Soc*. 2000;122(20):4996-4997.
24. Debad JD, Morris JC, Lynch V, Magnus P, Bard AJ. Dibenzotetraphenylperiflanthene: synthesis, photophysical properties, and electrogenerated chemiluminescence. *J Am Chem Soc*. 1996;118(1):2374-2379.
25. Wang Y, Yang J, Gong Y, Fang M, Li Z, Tang BZ. Host–guest materials with room temperature phosphorescence: tunable emission color and thermal printing patterns. *SmartMat*. 2020;1(1):e1006.
26. Dias FB, Bourdakos KN, Jankus V, et al. Triplet harvesting with 100% efficiency by way of thermally activated delayed fluorescence in charge transfer OLED emitters. *Adv Mater*. 2013;25(27):3707-3714.
27. dos Santos PL, Dias FB, Monkman AP. Investigation of the mechanisms giving rise to TADF in exciplex states. *J Phys Chem C*. 2016;120(32):18259-18267.
28. Grüne J, Bunzmann N, Meinecke M, Dyakonov V, Sperlich A. Kinetic modeling of transient electroluminescence reveals TTA as an efficiency-limiting process in exciplex-based TADF OLEDs. *J Phys Chem C*. 2020;124(47):25667-25674.
29. Wang S, Zhang H, Zhang B, Xie Z, Wong W-Y. Towards high-power-efficiency solution-processed OLEDs: material and device perspectives. *Mater Sci Eng R Rep*. 2020;140:100547.
30. Li W, Li Z, Si C, et al. Organic long-persistent luminescence from a thermally activated delayed fluorescence compound. *Adv Mater*. 2020;32(45):e2003911.
31. Jinnai K, Nishimura N, Adachi C, Kabe R. Thermally activated processes in an organic long-persistent luminescence system. *Nanoscale*. 2021;13(18):8412-8417.
32. Tan S, Jinnai K, Kabe R, Adachi C. Long-persistent luminescence from an exciplex-based organic light-emitting diode. *Adv Mater*. 2021;33(23):e2008844.
33. Kumar S, Tourneur P, Adsetts JR, et al. Photoluminescence and electrochemiluminescence of thermally activated delayed fluorescence (TADF) emitters containing diphenylphosphine chalcogenide-substituted carbazole donors. *J Mater Chem C*. 2022;1(12):4646-4667.
34. Adachi C, Xie G, Reineke S, Zysman-Colman E. Editorial: recent advances in thermally activated delayed fluorescence materials. *Front Chem*. 2020;8:625910.
35. Endo A, Sato K, Yoshimura K, et al. Efficient up-conversion of triplet excitons into a singlet state and its application for organic light emitting diodes. *Appl Phys Lett*. 2011;98(8):083302.
36. Zhang Z, Crovini E, dos Santos PL, et al. Efficient sky-blue organic light-emitting diodes using a highly horizontally oriented thermally activated delayed fluorescence emitter. *Adv Opt Mater*. 2020;8(23):2001354.
37. Hirai H, Nakajima K, Nakatsuka S, et al. One-step borylation of 1,3-diaryloxybenzenes towards efficient materials for organic light-emitting diodes. *Angew Chem Int Ed*. 2015;54(46):13581-13585.
38. Hall D, Suresh SM, dos Santos PL, et al. Improving processability and efficiency of resonant TADF emitters: a design strategy. *Adv Opt Mater*. 2019;8(2):1901627.
39. Madayanad SS, Hall D, Beljonne D, Olivier Y, Zysman-Colman E. Multiresonant thermally activated delayed fluorescence emitters based on heteroatom-doped nanographenes: recent advances and prospects for organic light-emitting diodes. *Adv Funct Mater*. 2020;30(33):1908677.
40. Ishimatsu R, Matsunami S, Kasahara T, et al. Electrogenerated chemiluminescence of donor-acceptor molecules with thermally activated delayed fluorescence. *Angew Chem Int Ed*. 2014;53(27):6993-6996.
41. Huang P, Zhang B, Hu Q, et al. Polymer electrochemiluminescence featuring thermally activated delayed fluorescence. *Chemphyschem*. 2021;22(8):726-732.
42. Zeng Z, Huang P, Kong Y, et al. Nanoencapsulation strategy: enabling electrochemiluminescence of thermally activated delayed fluorescence (TADF) emitters in aqueous media. *Chem Commun*. 2021;57(43):5262-5265.
43. Zhang R, Tong F, Yang L, et al. Facile synthesis and efficient electrochemiluminescence of a readily accessible pyridopyrimidine. *Chem Commun*. 2018;54(71):9897-9900.
44. Adsetts JR, Chu K, Hesari M, Ma J, Ding Z. Absolute electrochemiluminescence efficiency quantification strategy exemplified with $Ru(bpy)^{3}_{2+}$ in the annihilation pathway. *Anal Chem*. 2021;93(33):11626-11633.
45. Hesari M, Ding Z. Spooling electrochemiluminescence spectroscopy: development, applications and beyond. *Nat Protoc*. 2021;16(4):2109-2130.
46. Yang L, Adsetts JR, Zhang R, et al. Determining absolute electrochemiluminescence efficiencies of two iridium complexes. *J Electroanal Chem*. 2022;906:115891.
47. Valenti G, Fiorani A, Di Motta S, et al. Molecular size and electronic structure combined effects on the electrogenerated chemiluminescence of sulfurated pyrene-cored dendrimers. *Chem Eur J*. 2015;21(7):2936-2947.
48. Rosenmund J, Doblhofer K. The effects of uncompensated solution resistance and rate of the homogeneous electron transfer reaction on electrochemiluminescence transients. *J Electroanal Chem*. 1995;396:77-83.

49. Tokel NE, Bard AJ. Electrogenerated chemiluminescence. IX. Electrochemistry and emission from systems containing tris (2,2'-bipyridine)ruthenium(II) dichloride. *J Am Chem Soc*. 2002;94(8):2862-2863.
50. Serevičius T, Komskis R, Adomėnas P, et al. Triplet–triplet annihilation in 9,10-diphenylanthracene derivatives: the role of intersystem crossing and exciton diffusion. *J Phys Chem C*. 2017;121(15):8515-8524.
51. Keszthelyi CP, Bard AJ. Electrogenerated chemiluminescence. XV. On the formation of excimers and exciplexes in ECL. *Chem Phys Lett*. 1974;24(2):300-304.
52. Tokel NE, Keszthelyi CP, Bard AJ. Electrogenerated chemiluminescence. X. Alpha, beta, gamma, delta-tetraphenylporphine chemiluminescence. *J Am Chem Soc*. 1972;94(14):4872-4877.
53. Tachikawa H, Bard AJ. Electrogenerated chemiluminescence. XII. Magnetic field effects on ECL in the tetracene-TMPD system; evidence for triplet-triplet annihilation of tetracene. *Chem Phys Lett*. 1973;19(2):287-289.

AUTHOR BIOGRAPHIES

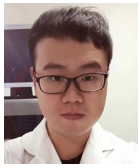

Liuqing Yang graduated from *Hunan University* with a Bachelor of Science in Chemistry in 2017. He is currently pursuing his doctoral degree with Professor Zhifeng Ding at *Western University*. His research interest focuses on the electrochemiluminescence study of novel luminescent materials as well as the synthesis, characterization, and application of graphene quantum dots, especially in light-emitting fields.

Yoann Olivier obtained a PhD from the *University of Mons* in 2008. From 2009 to 2013, he went on postdoctoral stays with Prof. Claudio Zannoni at the *University of Bologna* and Prof. Henning Sirringhaus at the *University of Cambridge*. From 2013 to 2019, he was a research associate at the *University of Mons* and recently joined in July 2019 the Chemistry and Physics departments of the *University of Namur* as a lecturer. His research interests deal with the understanding of electronic processes in organic conjugated (small molecule and polymers) and 2D materials using computational approaches.

Lihui Dong received her PhD degree from the School of Chemistry and Chemical Engineering at *Nanjing University* in 2011 under the supervision of Professor Lin Dong and was a postdoctoral fellow at *Guangxi University* with Professor Bin Li. She was a visiting scholar with Professor Zhifeng Ding at *Western University*. She is currently an associate professor at *Guangxi University*. Her research interests focus on the preparation and characterization of metallic oxide catalysts and their applications in the elimination of atmospheric molecular contaminants (NOx, CO, etc.)

Eli Zysman-Colman obtained his PhD in Chemistry from *McGill University* in 2003 with Prof. David N. Harpp. He then completed two postdoctoral fellowships, one in supramolecular chemistry with Prof. Jay Siegel at the *University of Zurich* and the other in inorganic materials with Prof. Stefan Bernhard at *Princeton University*. He joined the *Université de Sherbrooke* as an assistant professor in 2007. In 2013, he moved to the *University of St Andrews* where he is presently Professor of Optoelectronic Materials, Fellow of the RSC, and has been a holder of a Royal Society Leverhulme Trust Senior Research Fellowship.

Zhifeng Ding is a full professor of chemistry at *Western University*. He obtained his BSc in chemistry from *Southeast University*, MSc in coordination chemistry from *Nanjing University,* and PhD in electrochemistry from École Polytechnique Fédérale de Lausanne. He did postdoctoral research at the *University of Texas at Austin*. His research focuses on scanning electrochemical microscopy, ionic liquid electrolytes, solar cells, and electrochemiluminescence/electroluminescence. His achievements include the 2014 Science Distinguished Research Professor status, 2015 University Faculty Scholar recognition, 2017 Canadian Society for Chemistry McBryde Medal, and 2018 Ertl award.

SUPPORTING INFORMATION

Additional supporting information can be found online in the Supporting Information section at the end of this article.

How to cite this article: Yang L, Dong L, Hall D, et al. Insights into enhanced electrochemiluminescence of a multiresonance thermally activated delayed fluorescence molecule. *SmartMat*. 2022;1-14. doi:10.1002/smm2.1149